Metal-Binding and Nuclease Activity of an Antimicrobial Peptide Analogue of the Salivary Histatin 5[†]

Sonia Melino,*[,‡] Mariana Gallo,[§] Edoardo Trotta,[⊥] Francesca Mondello,[‡] Maurizio Paci,[§] and Raffaele Petruzzelli[∥]

Dipartimento di Scienze e Tecnologie Chimiche, Università di Roma "Tor Vergata", Rome, Italy, Istituto di Neurobiologia e Medicina Molecolare, CNR, Rome, Italy, Dipartimento di Malattie Infettive, Parassitarie ed Immunomediate, Istituto Superiore di Sanità, Rome, Italy, and Dipartimento di Scienze Biomediche, Università "G. D'Annunzio", Chieti, Italy

Received July 27, 2006; Revised Manuscript Received October 27, 2006

ABSTRACT: The salivary antimicrobial peptide histatin 5 is characterized by its cationic nature, structural flexibility, and the presence of two metal-binding sites (the ATCUN motif and a Zn-binding motif). These properties make this peptide a good model for the design of new drugs of low molecular weight. In this work, we have synthesized and studied a new peptide, an analogue of the histatin 5 named ATCUN-C16, which contains both metal-binding centers. The results show that our 20-residue-derived peptide preserves anticandidal activity and exhibits a higher propensity to assume a stable conformation in a hydrophobic environment than do histatin 5 and the C16 peptide that contains the 16 residues of the C-terminal part of histatin 5, although overall our peptide remains a flexible molecule. ACTUN-C16 was found to bind DNA in a gel retardation assay and to have a nuclease activity in the presence of copper and zinc ions and ascorbate. Its nuclease activity can be attributed to the synergistic action of oxidative and hydrolytic activities due to the Cu−ATCUN complex and to the zinc ion coordination, respectively. The results show a new property of this family of salivary peptides and suggest a novel use of this peptide as a small nuclease and biotechnological tool.

Human saliva contains non-immune proteins with potent antimicrobial activities that contribute to the innate host defense system in the oral cavity and have a wide spectrum of activities against bacteria and fungi. A component of this host non-immune defense system is represented by the salivary histatins, a family of histidine-rich basic proteins of human acinar cell origin, which possess *in vitro* candidastatic and candidacidal activities (*1*). Histatin 5 (Hst 5),[1] a proteolytic product of histatin 3, is the most potent of the histatin family members and has the highest anticandidal activity *in vitro* against *Candida glabrata*, *Candida krusei*, *Saccharomyces cerevisiae*, and *Cryptococcus neoformans* (*2*−*3*). The Hst 5, at physiological concentrations found in saliva (15−50 μM), induces 95% loss of viability of *Candida albicans*. Moreover, Hst 5 shows a pH dependent bactericidal and bacteriostatic activity against *Streptococcus mutans*, *Porfiromonas gengivalis*, and *Streptococcus mitis* (*4*−*5*). Hst 5 does not function as a classical pore-forming antibiotic, and the antimicotic mechanism of this salivary peptide is not yet exactly understood. It has been shown, however, that the Hst 5 killing is a multistep process. In fact, Hst 5 first binds to the heat shock protein Ssa1/2p (67−70 kDa protein) for the internalization inside the cytosol of the yeast cell (*6*−*10*). At present, two mechanisms have been proposed to explain its antimicrobial activity: the first mechanism acting through the production of reactive oxygen radical formation (ROS) at the level of mitocondria that seem to be the specific intracellular target (*8*, *11*) and the second mechanism through ATP and K^+ release (*12*) via interaction with the TRK1 potassium transporter (*13*). The structural characterization of the Hst 5 (*14*−*16*) has revealed the presence of two principal metal-binding motifs: the so-called ATCUN-motif (amino terminal Cu^{2+}- and Ni^{2+}-binding motif), represented by the first three N-terminal amino acids (Asp-Ser-His) (*17*−*18*), and the Zn-binding motif HEXXH in the C-terminal region. Moreover, spectroscopic and calorimetric studies have shown that Hst 5 presents high affinity for zinc ($K = 1 \times 10^{-5}$ M) and copper ions ($K = 2.6 \times 10^{-7}$ M) (*15*). The ATCUN motif occurs naturally in certain species of albumin (*17*) and has been demonstrated to bind Cu^{2+} ($K_D \sim 1.18 \times 10^{-16}$ M) and Ni^{2+} ($K_D \sim 10^{-17}$ M) with high affinity (*19*−*20*). Recently, it has been suggested that the ATCUN peptides may have a higher physiological relevance than merely serving as metal transport sites. In fact, the ATCUN sequence in human sperm proteamine P2a in metal-exposed individuals may provide a potential mechanism for carcinogenesis (*21*), whereas an ATCUN−peptide/ascorbate system was found to kill Ehrlich ascites tumor cells *in vitro* (*22*). In addition to this, the Ni/Cu−ATCUN peptide complex was also found to cleave DNA in the presence of co-reactants

[†] The work was partly supported by grants PRIN2004, "PRIN2005", and FIRB of Italian MIUR.

* Corresponding author. Telephone: #39-0672594449. Fax: #39-0672594328. E-mail: melinos@uniroma2.it.

[§] Dipartimento di Scienze e Tecnologie Chimiche.

[⊥] Istituto di Neurobiologia e Medicina Molecolare.

[‡] Departimento di Malattie Infettive.

[∥] Dipartimento di Scienze Biomediche.

[1] Abbreviations: Hst, histatin; MMPP, magnesium−monoperoxyphthalate; TAR RNA, trans-activation response region RNA; HMQC, Heteronuclear Multiple-Quantum Coherence; NOESY, Nuclear Overhauser Effect spectroscopy; TOCSY, Total Correlation spectroscopy; SDB, Sabouraud Dextrose broth; SUVs, small unilamellar vesicles.

10.1021/bi0615137 CCC: $33.50
Published on Web 12/01/2006

Table 1: Amino Acids Sequences of the Hst 5 and the Histatin-Derived Peptides

Histatin 5 (24 aa)	**DSHAKRHHGYKRKFHEKHHSHRGY**
Hst 5-Nter (10 aa)	**DSHAKRHHGY**
Hst 5A-Nter (10 aa)	**DSAAKRHHGY**
C16 (16 aa)	**GYKRKFHEKHHSHRGY**
ATCUN-C16 (20 aa)	**DSHAGYKRKFHEKHHSHRGY**

such as $KHSO_5$, MMPP, H_2O_2 (*23*−*25*), or by light activation in the presence of O_2 and in the case of peptide−Co^{2+} complexes (*26*). These complexes together with appropriate co-reactants have also demonstrated an ability to selectively modify the RNA and cleave both $tRNA^{Phe}$ and TAR RNA of HIV (*27*). Although, in the case of the Hst 5 peptide, the function of both metal sites has not yet been completely elucidated, it is probable that they play an important role in the physiological action of this salivary peptide.

In recent years, there has been a great deal of interest in the design of artificial nucleases, small molecular scissors that bind DNA at specific sequences of interest and are able to cleave it hydrolytically. These artificial peptidic-nucleases would have a wide applicability either as tools in molecular biology and therapy or as probes of the structure and function of nucleic acids. Recently, reactive peptides containing histidine residues for Zn^{2+} coordination were designed *de novo* to be flexible with a modest helicity (25% α-helix) and to behave as a DNA intercalator for delivering both the peptide and metal close to the DNA backbone (*28*). The properties of the cationic salivary peptide Hst 5, which contains two metal centers and has a high structural flexibility, make it a potential peptidic-nuclease. Thus, on the basis of the solution structure of the Hst 5 (*14*) and functional studies, we have synthesized the ATCUN-C16 peptide (Table 1), an analogue of the Hst 5 corresponding to the fusion of the N-terminal ATCUN sequence with the C-terminal segment (Table 1) containing the zinc-binding motif. The goals were first to analyze the correlation between the antifungal activity and the propensity to assume a more stable conformation of this salivary histidine-rich peptide and then to test its nuclease activity due to the presence of metal-binding motifs. The conformation in the solution of ATCUN-C16, consisting of 20 amino acid residues, has been investigated by CD and NMR spectroscopy. It reveals that the peptide is able to assume a more stable conformation in a hydrophobic environment than the natural Hst 5, although it conserves a high flexibility. This peptide shows the same antifungal activity of the Hst 5 indicating either that all the components important for the antifungal activity are present or that the higher propensity to assume an α-helix conformation does not increase this activity. The DNA-binding ability of the ATCUN-C16 peptide has also been analyzed, and the oxidative and hydrolytic DNA cleavage due to the cooperative action of two metal centers of the peptide has been found, providing a new insight into its function and its potential use as a nuclease.

MATERIALS AND METHODS

Peptide Synthesis. Synthetic peptides Hst 5 (NH_2−DSHAKRHHGYKRKFHEKHHSHRGY−COOH), Nter−Hst 5 (NH_2−DSHAKRHHGY), Nter−Hst 5A (NH_2−DSAAKRHHGY), C16 (NH_2−GYKRKFHEKHHSHRGY−COOH), (*29*) and ATCUN−C16 (NH_2−DSHAGYKRKFHEKHHSHRGY−COOH) (Table 1) were purchased from Peptide Specialty Laboratories GmbH (Germany). Analysis of the synthetic peptides by reverse phase high performance chromatography (RP-HPLC) and mass spectrometry revealed a purity >98%.

Antifungal Assay. The growth inhibitory activity was evaluated following the broth microdilution method by Helmerhorst et al. (*30*). A clinical isolate of *C. albicans* (SA40) and reference strains of *C. albicans* (ATCC 10231) were used throughout this study. *C. albicans* (SA40) was isolated from oropharyngeal swab from HIV-seropositive subject. The cell density of the suspensions was estimated by direct cell count using a Thoma camera. Serial dilutions of synthetic Hst 5 and ATCUN-C16 peptides were prepared in diluted SDB in 96-well polystyrene microtitre plates (Microtest, Becton Dickinson Labware, USA) to a final volume of 50 μL/well. To each well, 50 μL of the diluted yeast suspension was added. Growth and broth-sterility controls were present in the same plate covered with a plastic seal to minimize broth evaporation and were then incubated at 30 °C for 48 h. After this incubation period, the cells in each well were carefully resuspended and the OD_{620nm} was determined using a microtitre plate reader (Labsystem Multiskan MS, Dasit, Milan, Italy). The IC_{50} values were determined and found to correspond to the concentration of antifungal peptides that inhibited the maximum growth of that particular strain by 50%. Values were corrected for the absorbance of diluted broth.

Spectrophotometric Metal-Binding Characterization. The peptides were dissolved in water to a concentration of 0.5 mM. Copper or nickel chloride was added in a 1:1 molar ratio with the peptides. The pH of the solution was decreased or raised using 0.1 M HCl or 0.2 M NaOH, respectively, and the solutions were equilibrated for 30 min at each pH before the spectrophotometric measurements. The visible spectra of the peptide−metal complexes were acquired on a Perkin-Elmer (Lambda-Bio) spectrophotometer.

Circular Dichroism. CD measurements were performed at different percentages of 2,2,2-trifluoroethanol (TFE) using a Jasco 600 spectropolarimeter (Jasco, Tokyo, Japan) calibrated with camphor−sulfonic acid. CD spectra were obtained between 200 and 250 nm using a path length of 0.1 cm and between 600 and 300 nm using a path length of 1 cm, a time constant of 1.0 s, a 2 nm bandwidth and a scan rate of 2 nm/min, and at 20 or 50 mdeg sensitivity. The average was corrected by 4 scans of the solvent. Quartz cells (0.1−1 cm path length) sealed and controlled thermostatically were used for the far- and near-UV CD measurements, respectively. The samples for CD measurements, at different concentrations of TFE in the absence and in presence of Ni^{+2} ions, were prepared at 50 μM ATCUN-C16 peptide. The near-UV CD spectra were recorded at 300 μM ATCUN-C16 in 20 mM Tris−HCl buffer at different pHs and at an equimolar concentration of $NiCl_2$.

EPR Spectroscopy. X-band (9.4 GHx) electron paramagnetic resonance (EPR) spectra at 100 K were measured on an ESP300 Bruker spectrometer with a 100 kHz field modulation of 0.5 mT. A titration at different molar ratios of Cu/peptide (0, 0.5, and 1) was performed using a solution of 300 μM peptide in a 50 mM Hepes buffer, pH 7.2.

NMR Spectroscopy. The ATCUN-C16 peptide (10 mM) was dissolved in a 50% TFE-d_3-50% in water solution, pH 6.0. The spin systems of different amino acid residues in the peptide were identified using TOCSY, ^{1}H−^{13}C HMQC, and ^{1}H−^{13}C TOCSY−HMQC spectra, the last mentioned being very helpful due to the overlap of the signals. The sequential connectivity across the peptide was established using the NOESY spectra. The sequential NOE connections include NH_i−NH_{i+1}, $H_{\alpha i}$−NH_{i+1}, and $H_{\beta i}$−NH_{i+1} cross-peaks. The NMR experiments were performed at 25 °C using a Bruker Avance 400 spectrometer (Bruker, Milan, Italy) equipped with triple resonance probes incorporating self-shielded gradient coils. All the heteronuclear correlation experiments were carried out at natural abundance. Pulsed field gradients were appropriately employed to achieve suppression of the solvent signal and spectral artifacts. Quadrature detection in the indirectly detected dimensions was obtained using the States−TPPI method (*31*) or the echo−antiecho method; the spectra were processed on Silicon Graphics workstations (Silicon Graphics, Milan, Italy) by the NMRPipe software (*32*) and analyzed using NMRView (*33*). All the proton and carbon resonances were assigned by 2D spectra: TOCSY (mixing time 60 ms) to identify the spin systems, ^{1}H−^{13}C HMQC, (*34*) and ^{1}H−^{13}C HMQC−TOCSY (with a mixing time of 40, 60, and 80 ms) to assist with cross-peaks assignment, NOESY (with a mixing time of 0.150 and 0.250 s), according to the sequential assignment method. The values of $^1J_{C_\alpha H_\alpha}$ coupling constants were measured from the in-phase splitting patterns of the C_α−H_α cross-peaks in the HMQC spectra without carbon decoupling.

DNA Binding. Plasmid DNA (pQE30-rhdA) was isolated from *E. coli* using Plasmid Mini Kit (Sigma-Aldrich, Milan, Italy). The gel retardation assay was performed by mixing the plasmid DNA (500 ng) with increasing amounts of peptides (300 ng to 2, 4 μg) in 50 mM Tris pH 7.5. After incubation for 2 min at room temperature, the samples were electrophoresed on 1% agarose gel in TAE buffer for 80 min at 70 V and stained with ethidium bromide. The pDNA was incubated with ATCUN-C16 or with the Zn−Cu−ATCUN-C16 complex in a pDNA:peptide ratio of 1:10 w/w for 10 min at room temperature. The SmaI restriction enzyme (Fermentas, M-Medical, Milan, Italy) was added to the solutions (1U/μg), and after 1 h at 30 °C, the samples were electrophoresed on 1% agarose gel.

Plasmid Cleavage. The plasmid DNA cleavage reactions were performed in a total reaction volume of 20 μL containing a cleavage agent and 54 μg of the plasmid DNA (4500 base pairs). Final concentrations were 50 mM Tris−HCl (pH 7.5, sterile-buffer filtered), 100 μM ascorbic acid, 10 and 100 μM peptide, and $CuCl_2$ solution in a 1:1 molar ratio with the peptides. After equilibration of DNA−metal−peptide solutions for 10 min at room temperature, the reactions were initiated by the addition of the ascorbic acid. The reactions were carried out at 37 °C and were terminated by addition of 2 μL of 6X gel loading buffer (5% glycerol, 0.125% bromophenol blue, 25 mM EDTA) and placed on ice before electrophoresis in 1% agarose gel in the TAE buffer. Samples were run for 120 min at 70 V and stained with ethidium bromide.

HPLC Analysis of the DNA Cleavage. The cleavage of the ssDNA was monitored using RP-HPLC analysis (LC-10AVP Shimadzu Italia, Milan, Italy). A 47-mer oligonucleotide (5′-CTGTCCCGGGAACTCCTGGTGCCGCGCG-GCAGCCCCGTCGCACTCAG-3′) was treated with Cu−Zn−ATCUN-C16−complex and a 10-fold excess of ascorbate in 50 mM Tris−HCl buffer, pH 7.4, at 37 °C for 1.30 h. Subsequently, the reaction mixture was loaded onto a Brownlee C-18 column equilibrated with 0.1 M NH_4Oac, pH 6.8 (solvent A). The products were eluted with an acetonitrile (solvent B) gradient (0−5 min, 100% A; 5−45 min, 40% B; 45−50 min, 40% B; and 50−75 min 90% B in A) and monitored at 254 nm.

RESULTS

Antifungal Activity of the ATCUN-C16 Peptide. The antifungal activity of the ATCUN-C16 peptide against two fungal strains of *C. albicans* was assayed, as described in Materials and Methods. Hst 5 and ATCUN-C16 peptides showed the same antifungal activity *in vitro*. The IC_{50} values obtained with *C. albicans* strains were in the range 6.25−25 μg peptide/mL. Generally, MFCs (minimum fungicidal concentrations) and IC_{50} values coincided in azoles susceptible fungal strains for Hst 5 and ATCUN-C16 (6.25 μg/mL).

Spectroscopic Characterization of the Metal-Binding Site. The characterization of the metal binding to the peptides was performed by UV−vis spectroscopy (Figure 1 and 2). The binding of Cu^{2+} to the peptide Nter−Hst 5 shows an absorption maximum at 525 nm in the pH range 5.0−10.50 (Figure 1A). The absorption maximum at 525 nm that is reached at a low pH (5.2) and is maintained through a rather wide range of pH values is indicative of a copper−ATCUN complex (*35*). Proteins that do not coordinate copper show a broad maximum near 600 nm, which eventually shifts to 525 nm only at very high pH. In contrast, the optical spectra of Ni^{2+} in the presence of Nter−Hst 5 clearly show a maximum at 420 nm (Figure 1B), which appears at pH 5.0 and is maintained up to pH 10. These results clearly demonstrate the presence of metal binding to the ATCUN motif, which involves the α-amino nitrogen, two intervening peptide nitrogens, and the imidazole nitrogen of the histidine present in the third position, as already reported in human serum albumin (*17*−*18*). Moreover, the spectra of the whole ATCUN-C16 peptide in the presence of nickel ions show the presence of a maximum at 420 nm at the pH range 5−7, as shown in Figure 2. On the contrary, the Nter−Hst 5A peptide is able to bind metal ions only at pH values higher than 9 (data not shown). Further structural features of the binding of metals to the ATCUN-C16 peptide have been obtained by CD studies. Figure 3 shows the near-CD spectra of the ATCUN-C16 recorded in the presence of the equimolar concentration of nickel ions at different pH values (pH 3−6). The dichroic measurements of the ATCUN-C16 peptide, recorded at the pH values 5 and 6, show two dichroic bands at 480 and 410 nm that are characteristic of the distorted square-planar geometry of the Ni^{2+} ions in a peptidic Ni(II)N4 site involving a His residue (*36*). EPR

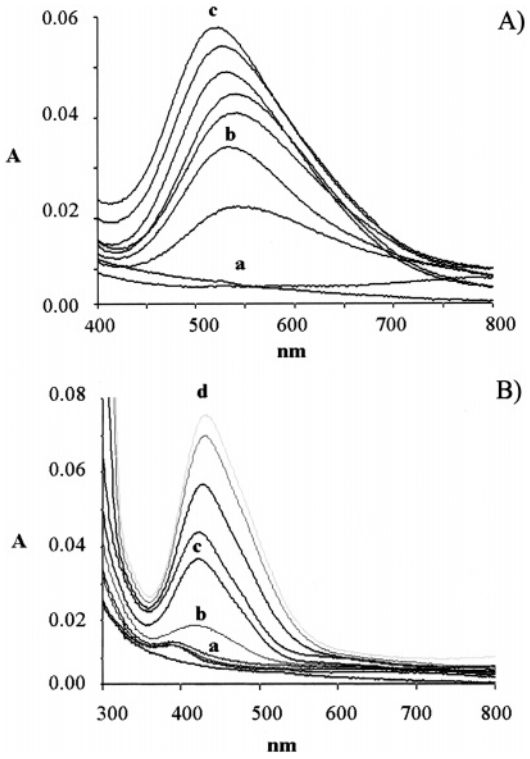

FIGURE 1: Optical spectra of Cu^{2+} and Ni^{2+} binding to Nter-Hst 5 peptide. (A) Optical spectra of 0.5 mM Nter-Hst 5 peptide in the presence of an equimolar amount of Cu(II) as a function of pH, in the range 3.0−11.0. For clarity, only three pH values are reported: pH 3.0 (a), pH 5.4 (b), and pH 11.0 (c). (B) Visible region of spectra of 0.5 mM Nter-Hst 5 peptide in the presence of an equimolar amount of Ni^{2+} as a function of pH, in the range 3.0−11.0. For clarity, only four pH values are reported in the figure: pH 3.4 (a), pH 6.0 (b), pH 7.4 (c), and pH 11.0 (d).

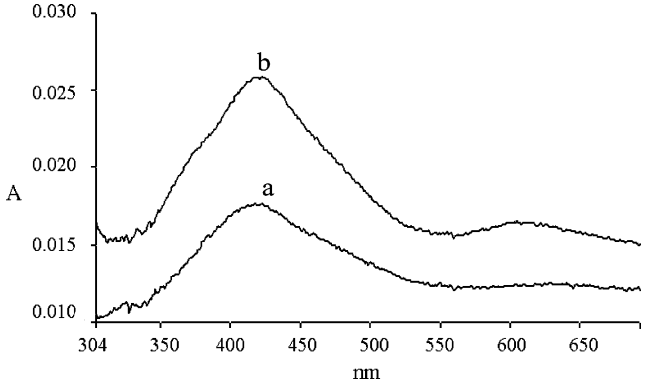

FIGURE 2: Optical spectra of Ni^{2+} binding to the ATCUN-C16 peptide. Visible region of spectrum of 0.5 mM ATCUN-C16 peptide in the presence of an equimolar amount of Ni^{2+} as a function of pH. The spectra were measured at pH 5.5 (a) and pH 6.6 (b).

spectra of the Cu−ATCUN-C16 complex in frozen solution were performed at different molar ratios of Cu/peptide (0, 0.5, and 1) to better characterize the copper-binding site. The EPR spectrum of the Cu−ATCUN-C16 complex with 1 equiv of Cu^{2+} is shown in the Supporting Information. The spectrum shows a unique copper coordination site, and the values $A_{\|}$, $g_{\perp}$, and $g_{\|}$ were, respectively, 208.6, 2.42, and 2.176 for the species with Cu/peptide molar ratios of 0.5 and 1. These values are consistent with those of Cu−ATCUN complex reported in the literature (*37*, *38*), indicating that the complex has a square-planar geometry characteristic of the copper binding to the ATCUN motif, and in these

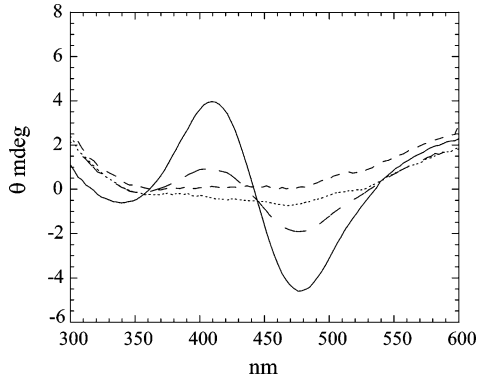

FIGURE 3: Near-UV CD spectra of ATCUN-C16. ATCUN-C16 (300 μM) at different pHs in absence (---) and in the presence of an equimolar concentration of $NiCl_2$: (•••••) pH 3.3; (– –) pH 5.5, and (—) pH 6.6.

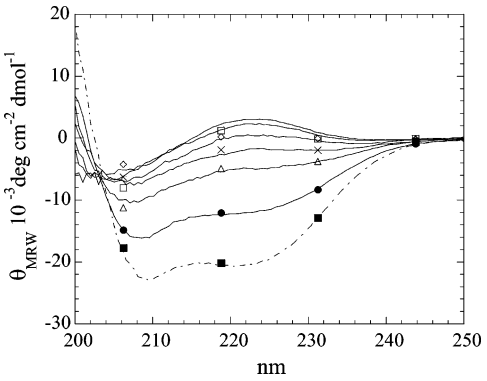

FIGURE 4: CD spectra of ATCUN-C16 as a function of TFE concentration. ATCUN-C16 peptide (50μM) in water (—); 10%-(–□–); 20%(–◇–); 30%(–×–); 50%(–△–); 80% (–●–); and 100% TFE (–■–).

conditions, the other residues of the peptide do not seem to affect the coordination structure of this complex.

Structural Characterization of the ATCUN-C16 Peptide by CD and NMR Spectroscopy. The dichroic profiles of the ATCUN-C16 peptide in water solution or in a water/2,2,2-trifuoroethanol (TFE) mixture are reported in Figure 4. The peptide, likely Hst 5, assumes a random coil conformation in water; an increase in the TFE concentration induces a substantial enhancement in the negative ellipticity at 208 and 222 nm, indicating the formation of an α-helix. The helix conformation, in a 50% TFE v/v mixture, was estimated to correspond to 25% of the length of the peptide chain, using the K2d program (http://kal-el.ugr.es/k2d/k2d.html) (*39*−*40*). The ATCUN-C16 peptide shows a higher conformational stability than the Hst 5 peptide. In fact, at 50% TFE v/v, the mean residue ellipticity at 222 nm is −5174 deg cm^2 $dmol^{-1}$, and the Hst 5 only at 90% TFE v/v has a mean residue ellipticity at 222 nm of −5420 deg cm^2 $dmol^{-1}$, as reported in a previous paper (*14*). Also, the C16 peptide (*29*) shows a lower propensity to assume a helix conformation in TFE than the ATCUN-C16 peptide (see Figure 5), indicating that the presence of the first 4 residues contributes to the stabilization of the helix in the C-terminal region. The ^1H, ^{15}N, and ^{13}C NMR signals of the ATCUN-C16 peptide in a 1:1 d_3-TFE/H_2O mixture at pH 6.0 were assigned through 2-D NMR spectra. Figure 6A shows the NH−H_α region of the NOESY spectrum; Figure 6B shows the $^{13}C_\alpha$−$^1H_\alpha$ region of the ^1H−^{13}C HMQC spectrum of the ATCUN-C16 peptide. The chemical shift analysis of the H_α, C_α, and C_β resonances

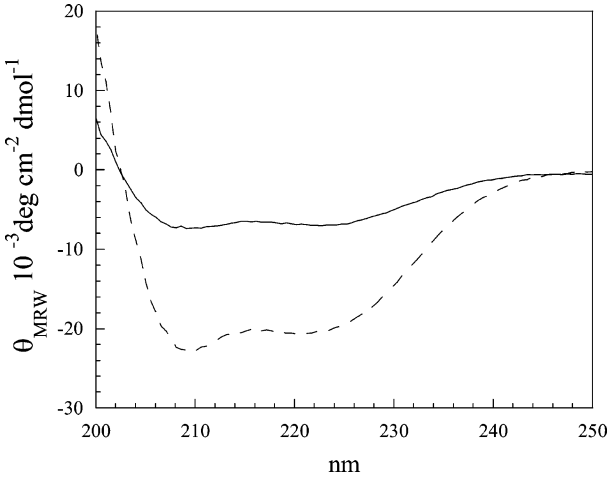

FIGURE 5: Comparison of the near-UV CD spectra of ATCUN-C16 and C16. The two peptides were at concentration a 50 μM in 100% TFE, (—) C16, and (- -) ATCUN-C16 peptide.

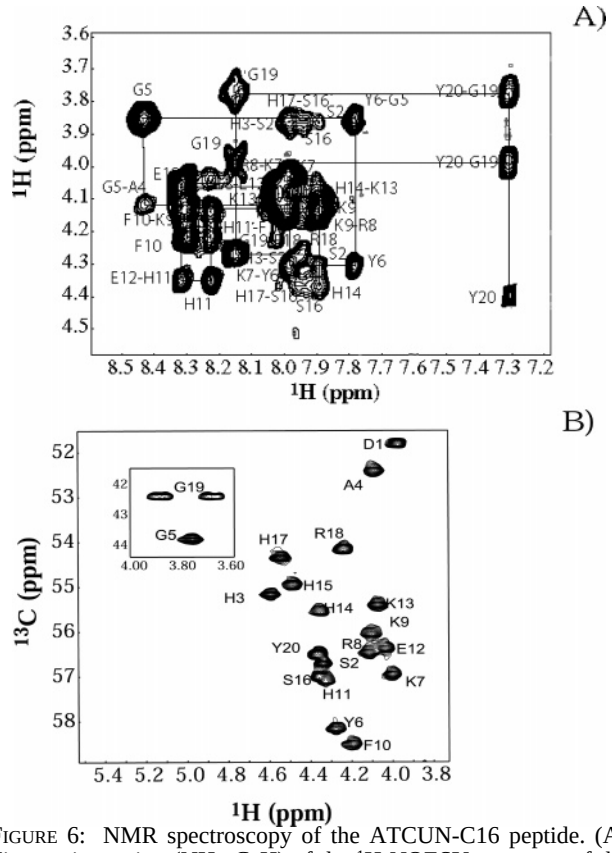

FIGURE 6: NMR spectroscopy of the ATCUN-C16 peptide. (A) Fingerprint region (NH−C_αH) of the ^{1}H-NOESY spectrum of the 10 mM ATCUN-C16 peptide. The sequential αN(i, i+1) connectivities are shown with a solid line (α-protons of residues H3, H15, and H17, whose resonances were close to the water signal, were not observed in the spectrum). (B) Region of the [^{13}C,^{1}H]−HMQC spectrum of ATCUN-C16. The assignment of C_α−H_α cross-peaks is shown. The inlet shows the C_α−H_α cross-peaks corresponding to the glycine residues (G5 and G19).

(*41*) of the ATCUN-C16 peptide at 25 °C indicates that the peptide adopts an α-helix conformation from Y6 to S16 (Figure 7A). Negative variations with respect to reference random coil values for H_α and C_β, and positive values for C_α, are indicative of an α-helix conformation. The presence of an α-helix from Y6 to S16 is supported by the values of the $^1J_{C_\alpha H_\alpha}$ coupling constants (Figure 7B). The α-helical residues have on average relatively large $^1J_{C_\alpha H_\alpha}$ values (146.5 ± 1.8 Hz), showing positive deviations with respect to random coil values (*42*). In particular, the α-helix propensity is weaker in the C-terminal region from residue H11 to the end of the tract. The chemical shift deviations from random coil values are less pronounced for these residues. However, the corresponding $^1J_{C_\alpha H_\alpha}$ values are still consistent with an α-helix conformation in this zone. Also, in the cases where evaluation was possible, the NOE pattern is consistent with an α-helix conformation in the region from Y6 to S16 (Figure 7C). The NH_i−NH_{i+1} NOEs characteristic of an α-helix were observed. Additionally, in some cases, where the overlap of signals did not prevent it, relatively strong $H_{\alpha i}$−NH_{i+3} and $H_{\alpha i}$−$H_{\beta i+3}$ and medium $H_{\alpha i}$−NH_{i+1} cross-peaks in the NOESY spectrum could be observed. In contrast, the N-terminal region of the peptide does not present a characteristic set of secondary chemical shifts corresponding either to an α-helix or to a β-sheet. We also analyzed if conformational changes were induced by the presence of the metal ions. The dichroic spectrum of the Ni^{2+}−ATCUN-C16

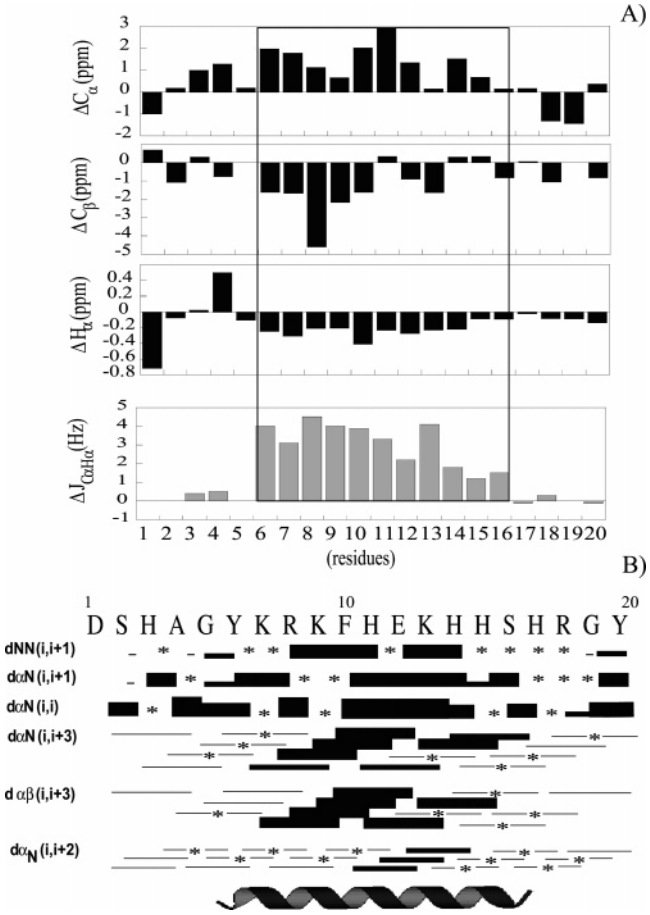

FIGURE 7: Structural characterization of the ATCUN-C16 peptide in 50% d_3-TFE/ water mixture. (A) Plot of the chemical shift differences between the observed resonances and values found in a random coil conformation, $\Delta\delta = \delta_{(obsd)} - \delta_{(random\ coil)}$ for $^1H_\alpha$, $^{13}C_\alpha$, and $^{13}C_\beta$. (B) Plot of the constant coupling $^1J_{C_\alpha H_\alpha}$ differences in Hz between observed and random coil values, $\Delta^1J_{C_\alpha H_\alpha}n = {}^1J_{C_\alpha H_\alpha(obsd)} - {}^1J_{C_\alpha H_\alpha\ (random\ coil)}$. (C) Summary of sequential and medium-range NOE data obtained from the NOESY spectra of ATCUN-C16. Strong (thick lines), medium (medium lines), and weak (thin lines) NOEs, corresponding to the intensity of the cross-peaks, are indicated. The asterisks represent the NOEs that cannot be assigned due to the signal overlapping or because signals were missing in the spectrum. The tract in α-helical conformation is shaded on the plots and depicted below the graphs.

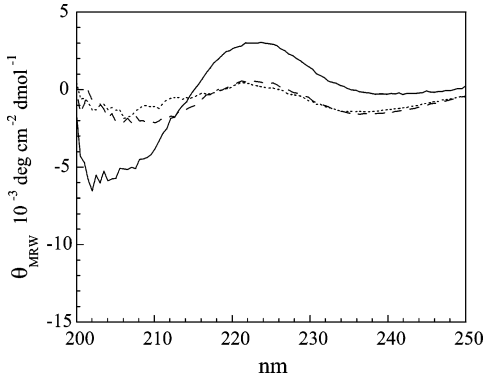

FIGURE 8: Far-UV CD spectra of the ATCUN-C16 in 50% TFE, at pH 5.9, in the absence (—) and presence of the equimolar concentration of nickel ions (---) and nickel plus zinc ions (– –).

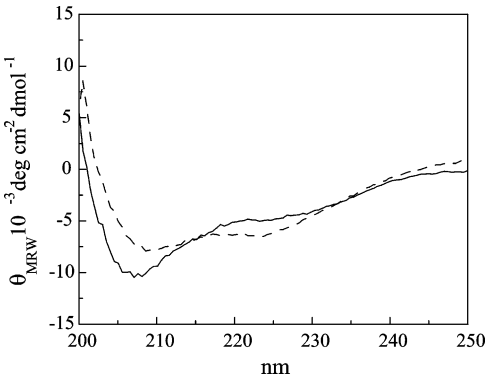

FIGURE 9: Far-UV CD spectra of the 50 μM ATCUN-C16 in 50% TFE in the presence (---) and absence (—) of Ni^{2+} ions.

complex in the far UV (Figure 8) shows a conformational variation of the peptide in the presence of nickel; in particular, 9% percent of the helix was calculated by deconvolution of the spectrum using the K2d program (*39*−*40*). The following addition of the zinc ions to the Ni−ATCUN-C16 complex showed only a small change in the CD spectrum. Figure 9 shows the far-UV CD spectrum of the ATCUN-C16 in 50% TFE in the presence and absence of the equimolar concentration of nickel ions. In the presence of Ni^{2+}, the far−UV spectrum of the ATCUN-motif is dominated by the contribution of the α-helix with prominent bands at 222 and at 208 nm, whereas in the absence of the metal ions the band at 208 nm is more negative than the band at 222 nm. It is worth recalling that in the 3_{10}-helix the $n-\pi^*$ transition exhibits a drastically reduced intensity with respect to that of the $\pi-\pi^*$ transition and tends to undergo a modest blue shift (*43*). Values for the $[\theta]_{222}/[\theta]_{208}$ ratio close to unity are seen as typical of the α-helix; a value of 0.15−0.40 is considered diagnostic for the 3_{10} helical conformation. In our case, the $[\theta]_{222}/[\theta]_{208}$ ratio is 0.5 in the absence and 0.8 in the presence of Ni^{2+}, indicating a better stabilization of the right-handed α-helix in the case of the Ni^{2+}−ATCUN-C16 complex (*44*). Moreover, the analysis of the spectra using the K2d program (*39*−*40*) shows that the presence of the Ni^{2+} ions induces an increase of 7% of the α-helix conformation. The change of conformation produced by Ni^{2+} was also observed by NMR spectroscopy. Figure 10 shows the overlapping of the $C_\alpha-H_\alpha$ region of the $[^{13}C,^1H]$−HMQC spectra of ATCUN-C16 in the absence and presence of Ni^{2+}. There is a significant chemical shift perturbation induced by nickel in the $C_\alpha-H_\alpha$ cross-peaks

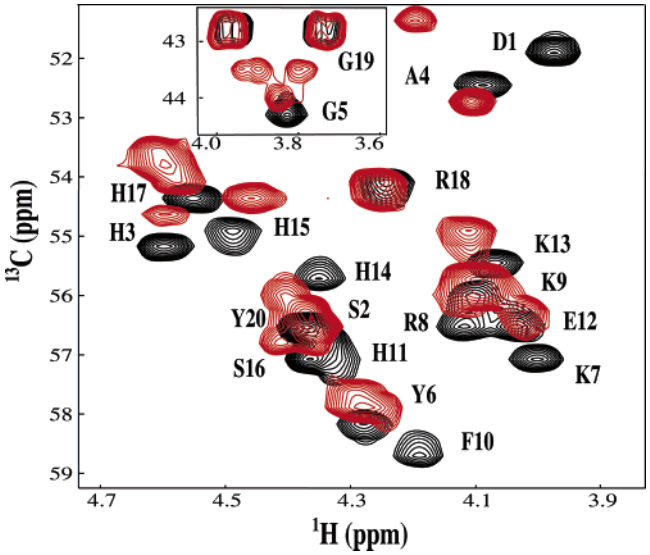

FIGURE 10: $^1H-^{13}C$ HMQC spectra of 1 mM ATCUN-C16 peptide in the absence (shown in black) and presence (shown in red) of an equimolar concentration of $NiCl_2$ in 50% d_3-TFE/water mixture at pH 6.0.

corresponding not only to the residues of the N-terminal tract (where the Ni^{2+} binds) but also in the rest of the peptide sequence, with the exception of the C-terminal residues R18, G19, and Y20. The TOCSY spectrum of the Ni−ATCUN-C16 complex shows a better spectral dispersion of the resonances than that in the absence of nickel ions; this may be indicative of a conformational stability in the presence of the metal ions (data not shown). All these results are in agreement with the α-helical stabilization induced by Ni^{2+} observed by CD and suggest that the α-helical tract in the ACTUN-C16 peptide seems to be involved.

The Metal−ATCUN-C16 Complex Binds and Cleaves the DNA. The ATCUN-C16 DNA-binding ability was evaluated in a gel retardation assay. Peptide was mixed with a fixed amount of plasmid DNA to obtain a w/w ratio of peptide/DNA of 0, 0.5, 1, 2, and 4, and the complexes were electrophoresed on agarose gel (Figure 11A). At a peptide/DNA weight ratio of 1, a fraction of the plasmid DNA remained at the origin (a_1 band), and this effect was more evident at higher peptide/DNA ratios. The ability of the SmaI restriction enzyme to cleave the pDNA in the presence or absence of the ATCUN-C16 peptide was also analyzed (Figure 11B). The SmaI enzyme has two recognition sites inside the pQE30-rhdA and normally is able to cleave this plasmid into two fragments of molecular weights of about 3900 (b_1 band) and 600 bp (b_2 band). The preincubation of the pDNA with the ATCUN-C16 peptide or with the Cu−Zn−ATCUN-C16 complex induces a reduction of the bands of the cleaved DNA and an evident DNA retardation shift (b_3 band), neither of which are found in case of preincubation with a peptide that does not bind the pDNA with high efficiency (data shown in Supporting Information). All these results show that ATCUN-C16 peptide has an intrinsic DNA-binding ability and can inhibit the interaction of DNA with other proteins. Moreover, the DNA binding of the peptide was studied by CD spectroscopy and an evident conformational change of the peptide in the presence of the pDNA was observed (data shown in Supporting Information).

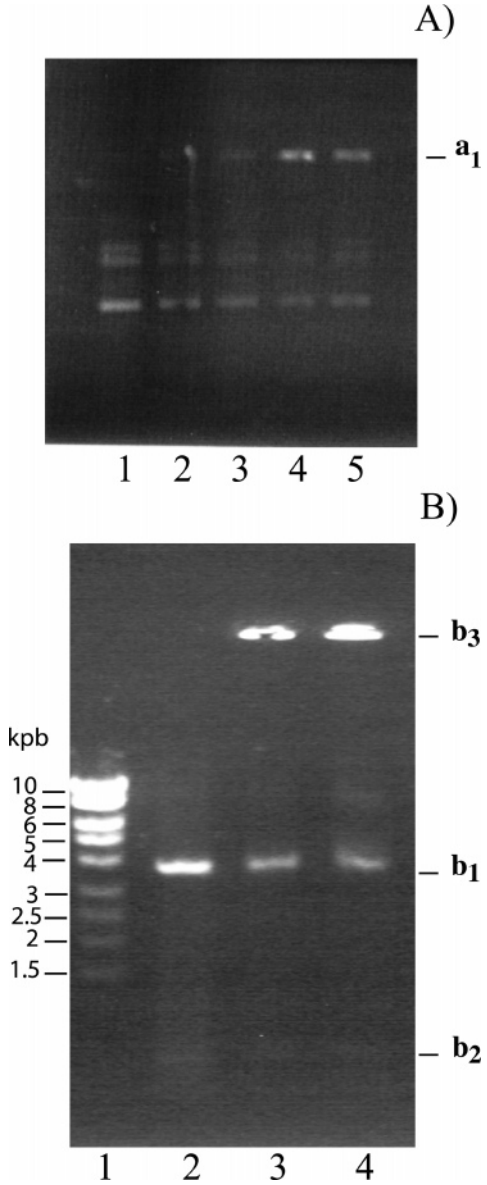

FIGURE 11: pDNA binding of the ATCUN-C16 peptide. (A) Gel retardation shift assay at different peptide/pDNA w/w ratios using 0.5 μg pQE30-rhda and 1% agarose gel. Lane 1 (0), lane 2 (0.5), lane 3 (1), lane 4 (2), and lane 5 (4). The a_1 band is due to the retardation shift effect of the peptide on the pDNA. (B) Agarose gel electrophoresis (1% agarose) of the 0.25 μg pQE30-rhdA after cleavage with SmaI (1U/μg) for 1 h at 30 °C in the absence (lane 2) and presence (lane 3) of the ATCUN-C16 peptide or the Cu−Zn−ATCUN-C16 complex (lane 4) in a ratio of pDNA/peptide of 1:10 w/w. The b_1 and b_2 bands correspond to the SmaI digest fragments of about 3900 and 600 bp, respectively. Molecular weight markers are shown in lane 1.

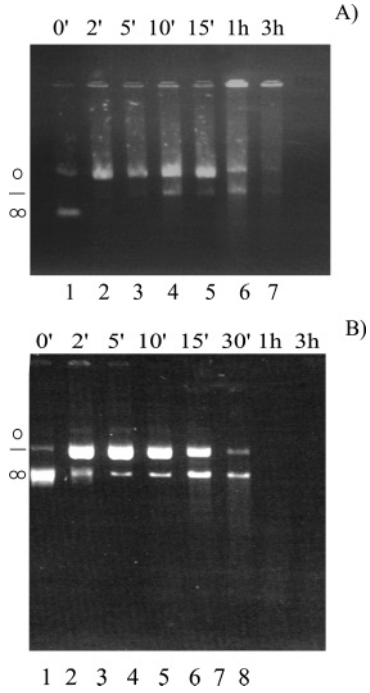

FIGURE 12: Agarose gel electrophoresis of pDNA treated with the ATCUN-C16 peptide in 50 mM Tris−HCl buffer, pH 7.5. (A) pDNA/ATCUN-C16 peptide mixture (ratio 1:1 w/w) in the presence of $CuCl_2$ and ascorbic acid at a molar ratio of peptide/Cu/ascorbate of 1:1:10 c/c/c incubated for 0 (lane 1), 2 (lane 2), 5 (lane 3), 10 (lane 4), 15 (lane 5), 60 (lane 6), and 180 (lane 7) min at 37 °C. (B) pDNA/ATCUN-C16 peptide mixture in the presence of $CuCl_2$, $ZnCl_2$, and ascorbic acid at a molar ratio of ATCUN-C16 peptide/Cu/Zn/ascorbate of 1/1/1/10 c/c/c/c incubated for 0 (lane 1), 2 (lane 2), 5 (lane 3), 10 (lane 4), 15 (lane 5), 30 (lane 6) 60 (lane 7), and 180 (lane 8) min at 37 °C.

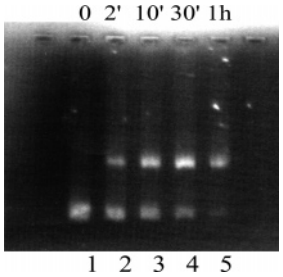

FIGURE 13: Nuclease activity of Cu−Hst5-Nter complex in the presence of ascorbic acid. Electrophoresed agarose gel (1% agarose) of 0.2 mg of pDNA in Tris−HCl buffer, pH 7.5, in the presence of 0.2 μg of peptide and an equimolar concentration of $CuCl_2$ with the peptide, after incubation, in the presence of ascorbic acid, at different times: 0, 2, 10, 30, and 60 min at 37 °C.

The DNA-binding ability was also observed for the Hst 5 peptide (data shown in Supporting Information). Considering that the Cu^{2+}/Ni^{2+}.X−X−His complex has the property of being a strong oxygen activator through the production of reactive oxygen species (*20*, *35*, *45*), we evaluated experimentally if these peptides were able to induce DNA cleavage. This motif cleaves the DNA by generating a nondiffusible oxidant that results in deoxyribose-centered damage depending on the presence of the L-ascorbic acid or monoperoxyphthalic acid (*20*, *35*, *45*). The Cu−ATCUN-C16 complex cleaves the pDNA; a rapid degradation of the supercoiled pDNA was found to produce nicked pDNA in the presence of ascorbate at 37 °C (shown in Figure 12A). After 5 min, a band corresponding to the linear form of the pDNA was observed and the incubation for 1 h induced a decrease in the intensity of the pDNA bands. The appearance of a band on the top of the gel over time is indicative of the formation of an aggregate, probably due to the formation of a complex between the linear form of the DNA and the Cu−peptide complex. The nuclease activity of the Cu−Hst 5-Nter peptide was analyzed in the presence of ascorbate; the time course of the DNA cleavage is shown in the Figure 13. The nicked band of the pDNA was found after 2 min of incubation at 37 °C, and a gradual reduction of the supercoiled pDNA occurred. However, no linear pDNA was observed during these incubation times. Thus, the Cu−ATCUN-C16 complex

shows a higher nuclease activity than the Cu−Hst 5-Nter complex due to its intrinsic characteristics; i.e., higher content of basic amino acids is able to confer a higher capability to interact with the dsDNA. An increase in the nuclease activity of the metal−peptide complex was found in the presence of Zn^{2+} ions. In fact, the time course of the nuclease activity was performed in the presence of the Cu−ATCUN-C16 complex, zinc ions, and ascorbate (Figure 12B); after 2 min, the supercoiled degradation of the pDNA and the increasing of the nicked form of the pDNA both became clearly visible. Over time, an increase of the band corresponding to the linear pDNA was observed. Both the pDNA forms (nicked and linear) were degraded after 30 min of incubation at 37 °C until a complete cleavage of the pDNA was obtained after 1 h of incubation. In this case, the aggregate form of the pDNA was not visible and it is possible to suppose that the cleavage of the DNA was due to either an oxidative or hydrolytic mechanism. We also probed if DNA damage occurred in the presence of ATCUN-C16 and zinc ions. In this case, a pDNA hydrolytic activity of the Zn−ATCUN-C16 was not evident also after 20 h of incubation at 37 °C; in contrast, an increase in the intensity of the gel top band was clearly visible (data shown in Supporting Information). Thus, the zinc ions seem to enhance the interaction of the peptide−DNA during the time, but in the absence of the Cu/Ni−ATCUN complex, which is known to bind the DNA minor groove (*46*), very long incubation times are necessary to obtain a pDNA hydrolysis. In addition, the ssDNA-cleavage activity of the ATCUN-C16 peptide was analyzed by RP-HPLC. A 47-mer oligonucleotide (1 nmol) was mixed with 5 nmol of peptide, previously incubated in the presence of copper and zinc ions at equimolar concentration. The addition of an excess of ascorbate induced a rapid degradation of the oligonucleotide, as shown in the Figure 14. In fact, the RP-HPLC analysis of the solution after incubation in the presence of ascorbic acid shows a reduction in the intensity of the peak corresponding to the oligonulceotide and an increase in the injection peak probably due to the oligonucleotide degradation.

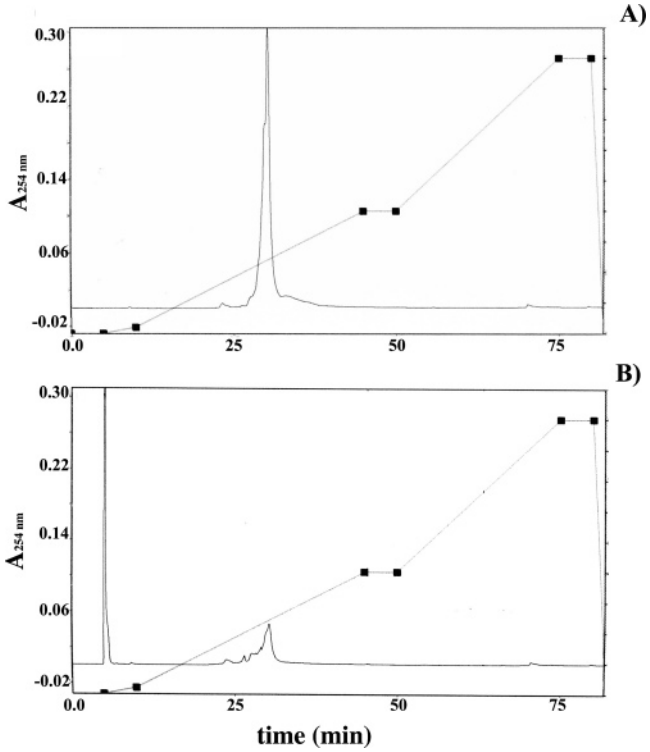

FIGURE 14: HPLC of 1 nmol of 47-mer oligonucleotide in the presence of 5 nmol of ATCUN-C16 and $CuCl_2$, $ZnCl_2$, and ascorbate at the molar ratio 1:1:1:5 at time 0 (A) and after 1.30 h of incubation at 37 °C (B).

DISCUSSION

Although the physiological role of the salivary histatin peptides remains unclear, peptides of this class are widely studied for their remarkable antimicrobial activity. Knowledge of their multiple functions may not only result in an understanding of the mechanism of the antimicrobial activity of the peptides, but it may also be a starting point for the design of potent antimicrobial peptides with relevant therapeutic applications. Moreover, the characteristic presence of two metal-binding sites (in particular, the ATCUN motif, the cationic nature, and the high flexibility of the peptide Hst 5) makes it a good model for either the design of new artificial nucleases or low molecular weight drugs. The delivery of metal ions to DNA is a common strategy for the hydrolysis of the phosphodiester bond. Thus, in the last years, dinuclear metal complexes have been synthesized and studied for DNA cleavage by double-strand cutting (*47*−*48*). We have synthesized the ATCUN-C16 peptide, which is shorter than the Hst 5 and conserves both metal-binding motifs present in the Hst 5. A characterization of the Ni/Cu binding of this peptide by several spectroscopic techniques has been presented here, although a detailed structural analysis will be done to establish the fine structure of the Zn−Cu/Ni−ATCUN-C16 complex. The structural characterization of the peptide, performed by CD and NMR spectroscopies, reveals that it shows a higher propensity to assume an α-helix conformation in a hydrophobic environment than the natural peptide analogue does. In fact, the ATCUN-C16 peptide adopts an α-helix conformation from the Y6 to S16 residues at 50% TFE v/v, and 25% of helix of the ATCUN-C16 peptide at the same conditions was estimated by deconvolution of its CD spectrum. On the contrary, the Hst 5 and C16 peptide show a similar percentage of the α-helix only reaching the 90% TFE v/v (*14*). Moreover, an α-helical conformation was detected from Y6 to S16 (corresponding to 50% of the peptide length) in the 50% TFE mixture by NMR spectroscopy. For ATCUN-C16, the data indicate the presence of a flexible helix. In fact, the deviation observed in chemical shifts and in coupling constants with respect to the random coil values are characteristic of an α-helix conformation, but the values are not as large as those observed in stable helical conformations. This indicates that the structured ATCUN-C16 peptide conserves a residual flexibility that seems to be a peculiar structural characteristic of the antimicrobial peptide Hst 5. Preliminary data on the antifungal activity, here reported, show that this peptide presents as much candidacidal activity as that of the natural peptide. This indicates that the stabilization of the α-helix conformation is substantially not relevant to its antifungal properties. These data are in agreement with the studies of Brewer et al. (*49*), which designed a cyclic histatin peptide more potent than Hst 5 against *S. cerevisiae* cells, concluding that the improvement in activity could be almost certainly associated to the stabilization of the bioactive conformation of histatin but that helicity was not an important factor for

antifungal activity. In our case, the enhancement of the structural stability was induced without placement of a disulfide bond, which produces a rigidity of the cyclic peptide; therefore, the mechanism of action of our peptide could be more similar to that of the Hst 5. Of note is that a further increase of the helix stability was induced by addition of the metal ions (Ni^{2+} and Zn^{2+}) at equimolar concentration as observed in our CD and NMR studies, indicating that the metal coordination can induce a significant difference in the interaction of the peptide with other macromolecules. Notably, the Ni^{2+} bound to the ATCUN motif may have an impact on the peptide conformation that extends for 5 or 12 residues beyond the coordination site, as described for the human protamine $HP2_1-15$ peptide (*50*), containing an ATCUN motif and a Zn-binding site. Moreover, in this case, the structuring effect of the metal coordination allows us to locate all positively charged side chains on one side of the molecule facilitating the DNA binding to the minor grove (*50*). Interestingly, another correlation between the helix content of synthetic peptides containing a Zn-binding motif and nuclease activity was observed (*28*). Recently, in fact, reactive peptides have been designed *de novo* so as to be flexible with a modest helicity, containing histidine residues for Zn^{2+} coordination, and to have a metallointercalator for delivering both peptide and metal to the DNA backbone (*28*). In this specific case, an intercalator coupled with a *de novo*-designed α-helix containing motif HXXXH has been shown to cleave both supercoiled plasmid and linear DNA substrates, although the DNA cleavage in the presence of Zn^{2+} ions was not site-specific (*28*). The DNA-cleavage activity and the helical content reached a maximum at a 1:1 molar ratio of Zn^{2+}, and a plasmid DNA hydrolysis was observed (*28*). Our results indicate that the ATCUN-C16 peptide binds the pDNA and in the presence of metal ions is able to induce cleavage of supercoiled pDNA. This nuclease activity was further enhanced in the presence of the zinc ions due to the Zn-binding region, which shows the higher propensity to assume a helical conformation.

However, DNA-binding and nuclease activity of the ATCUN-C16 peptide are also due to the ATCUN motif present at the N-terminal of the peptide. In fact, the Ni/Cu−ATCUN peptide complexes were shown to bind and cleave the DNA in the presence of co-reactants, such as mild reducing agents, suggesting that these complexes cause DNA cleavage through a mechanism involving C−4′H oxidation (*20*, *35*, *45*). Recently, it has been found that the ATCUN−Ni.Arg-Gly-His metallopeptide has a selective minor-groove binding and appears to be facilitated by the structure of the A/T-rich regions (AATT) (*46*). The His imidazole and N-terminal amino edge of the complex is inserted into the minor groove, forming distinct hydrogen bonds (*46*). On the basis of our results and the data reported in the literature, it is possible to suppose that DNA binding of the dimetal−ATCUN-C16 complex occurs at the minor groove of the dsDNA and that the binding of the zinc ions to the HEXXH motif leads to a better exposure of the side chains of the basic residues increasing the DNA-binding ability of the peptide. The cationic nature of this peptide favors the electrostatic interaction with the DNA backbone, enhancing the nuclease effect of the two metal-binding motifs. The nuclease activity of our peptide can therefore be attributed to the synergistic action of the Cu−ATCUN complex as oxidative activity and to the hydrolytic activity due to the zinc ion coordination. In fact, stable Zn^{2+} complexes are known to play an important role in phosphodiester cleavage enzymes such as the Klenow fragment DNA polymerase I, which is responsible for hydrolytic cleavage of the phosphodiester DNA backbone, and other hydrolytic enzymes containing Zn^{2+} in their active site (*51*−*52*). Moreover, the advantage of having two metal centers has been recently demonstrated by using dicerium and dicopper complexes that cleave both plasmid and linear DNA (*47*−*48*). The results obtained on the cleavage of the pDNA with the restriction enzyme show the competitive DNA-binding ability of the ATCUN-C16 and also suggest the possibility that this peptide is able to inhibit the interaction of the nucleic acids with other proteins. Moreover, the ability of this analogue of the Hst 5 to bind the dsDNA and the ssDNA could be related to the proposed mechanism of the Hst 5 to induce the cell cycle arrest of the *C. albicans* cells at the G1 state. In fact, the intracellular expression of the Hst 5 in *C. albicans* cells was correlated either to a rapid loss in the cellular volume or to the down-regulation of the expression in some proteins involved in the cellular cycle (*53*).

In conclusion, the results reported here demonstrate that the study of the interaction between metal ions and short peptides having important biological roles can be highly useful in designing new molecules with interesting properties and wide applicability as laboratory tools and therapeutic agents.

ACKNOWLEDGMENT

The authors are very grateful to Laura Garlando for taking part in the initial stages of this work and to Francesca Polizio for the EPR studies. We thank Gaio Paradossi for his help with the CD measurements and the use of his CD spectropolarimeter.

SUPPORTING INFORMATION AVAILABLE

Antifungal peptides activity against fungal strains determined by the broth microdilution method (Table 1). Two tables containing the $^1J_{C_\alpha H_\alpha}$ values and the ^1H and ^{13}C chemical shifts assignments of the ACTUN-C16 peptide in a 1:1 TFE/H_2O solution at 25 °C and pH 6.0 (Table 2 and 3). CD spectra of the peptide with or without the plasmid DNA (Figure 1). Electrophoresed agarose gels showing the pDNA after cleavage with SmaI in the presence of a peptide (that shows low ability to bind the DNA (Figure 2)) and the pDNA interaction with Hst 5 (Figure 3). Electrophoresed agarose gels of the pDNA incubated with the Zn−ATCUN-C16 complex (Figure 4) and with Ni−ATCUN-C16 in the presence of MMPP (Figure 5). X-band EPR spectrum of the Cu−ATCUN-C16 complex is shown in the Figure 6. This material is available free of charge via the Internet at http://pubs.acs.org.

REFERENCES

1. Oppenheim, F. G., Xu, T., McMillian, F. M., Levitz, S. M., Diamond, R. D., Offner, G. D., and Troxler, R. F. (1988) Histatins, a novel family of histidine-rich proteins in human parotid secretion. Isolation, characterization, primary structure, and fungistatic effects on *Candida albicans*, *J. Biol. Chem. 263*, 7472−7477.

2. Tsai, H., and Bobek, L. A. (1997) Human salivary histatin-5 exerts potent fungicidal activity against *Cryptococcus neoformans*, *Biochim. Biophys. Acta 1336*, 367−369.
3. Tsai, H., and Bobek, L. A. (1997) Studies of the mechanism of human salivary histatin-5 candidacidal activity with histatin-5 variants and azole-sensitive and -resistant Candida species, *Antimicrob. Agents Chemother. 41*, 2224−2228.
4. MacKay, B. J., Denepitiya, L., Iacono, V. J., Krost, S. B., and Pollock, J. J. (1984) Growth-inhibitory and bactericidal effects of human parotid salivary histidine-rich polypeptides on *Streptococcus mutans*, *Infect. Immun. 44*, 695−701.
5. Murakami, Y., Nagata, H., Amano, A., Takagaki, M., Shizukuishi, S., Tsunemitsu, A., and Aimoto, S. (1991) Inhibitory effects of human salivary histatins and lysozyme on coaggregation between *Porphyromonas gingivalis* and *Streptococcus mitis*, *Infect. Immun. 59*, 3284−3286.
6. Helmerhorst, E. J., Breeuwer, P., van't Hof, W., Walgreen-Weterings, E., Oomen, L. C., Veerman, E. C., Amerongen, A. V., and Abee, T. (1999) The cellular target of histatin 5 on *Candida albicans* is the energized mitochondrion, *J. Biol. Chem. 274*, 7286−7291.
7. Edgerton, M., Koshlukova, S. E., Lo, T. E., Chrzan, B. G., Straubinger, R. M., and Raj, P. A. (1998) Candidacidal activity of salivary histatins. Identification of a histatin 5-binding protein on Candida albicans, *J. Biol. Chem. 273*, 20438−20447.
8. Helmerhorst, E. J., van't Hof, W., Breeuwer, P., Veerman, E. C., Abee, T., Troxler, R. F., Amerongen, A. V., and Oppenheim, F. G. (2001) Characterization of histatin 5 with respect to amphipathicity, hydrophobicity, and effects on cell and mitochondrial membrane integrity excludes a candidacidal mechanism of pore formation, *J. Biol. Chem. 276*, 5643−5649.
9. Li, X. S., Reddy, M. S., Baev, D., and Edgerton, M. (2003) *Candida albicans* Ssa1/2p is the cell envelope binding protein for human salivary histatin 5, *J. Biol. Chem. 278*, 28553−28561.
10. Li, X. S., Sun, J. N., Okamoto-Shibayama, K., and Edgerton, M. (2006) *Candida albicans* cell wall SSA proteins bind and facilitate import of salivary histatin 5 required for toxicity, *J. Biol. Chem. 281*, 22453−22463.
11. Helmerhorst, E. J., Troxler, R. F., and Oppenheim, F. G. (2001) The human salivary peptide histatin 5 exerts its antifungal activity through the formation of reactive oxygen species, *Proc. Natl. Acad. Sci. U.S.A. 98*, 14637−14642.
12. Koshlukova, S. E., Lloyd, T. L., Araujo, M. W., and Edgerton, M. (1999) Salivary histatin 5 induces non-lytic release of ATP from *Candida albicans* leading to cell death, *J. Biol. Chem. 274*, 18872−18879.
13. Baev, D., Rivetta, A., Vylkova, S., Sun, J. N., Zeng, G. F., Slayman, C. L., and Edgerton, M. (2004) The TRK1 potassium transporter is the critical effector for killing of *Candida albicans* by the cationic protein, Histatin 5, *J. Biol. Chem. 279*, 55060−55072.
14. Melino, S., Rufini, S., Sette, M., Morero, R., Grottesi, A., Paci, M., and Petruzzelli, R. (1999) Zn^{2+} Ions Selectively Induce Antimicrobial Salivary Peptide Histatin-5 to Fuse Negatively Charged Vesicles. Identification and Characterization of a Zinc-Binding Motif Present in the Functional Domain, *Biochemistry 38*, 9626−9633.
15. Gusman, H., Lendenmann, U., Grogan, J., Troxler, R. F., and Oppenheim, F. G. (2001) Is salivary histatin 5 a metallopeptide?, *Biochim. Biophys. Acta 1545*, 86−95.
16. Grogan, J., McKnight, C. J., Troxler, R. F., and Oppenheim, F. G. (2001) Zinc and copper bind to unique sites of histatin 5, *FEBS Lett. 491*, 76−80.
17. Laussac, J. P., and Sarkar, B. (1984) Characterization of the Copper(II)- and Nickel(II)-Transport Site of Human Serum Albumin. Studies of Copper(II) and Nickel(II) Binding to Peptide 1−24 of Human Serum Albumin by ^{13}C and ^{1}H NMR Spectroscopy, *Biochemistry 23*, 2832−2838.
18. Rakhit, G., and Sarkar, B. (1981) Electron spin resonance study of the copper(II) complexes of human and dog serum albumins and some peptide analogs, *J. Inorg. Biochem. 15*, 233−241.
19. Lau, S. J., Kruck, T. P., and Sarkar, B. (1974) A peptide molecule mimicking the copper(II) transport site of human serum albumin. A comparative study between the synthetic site and albumin, *J. Biol. Chem. 249*, 5878−5884.
20. Long, E. C. (1999) Ni(II)·Xaa-Xaa-His Metallopeptide−DNA/RNA Interactions, *Acc. Chem. Res. 32*, 827−835.
21. Bal, W., Lukszo, J., and Kasprazak, K. S. (1996) Interactions of nickel(II) with histones: enhancement of 2′-deoxyguanosine oxidation by Ni(II) complexes with CH3CO-Cys-Ala-Ile-His-NH2, a putative metal binding sequence of histone H3, *Chem. Res. Toxicol. 9*, 535−540.
22. Kimoto, E., Tanaka, H., Gyotoku, J., Morishige, F., and Pauling, L. (1983) Enhancement of antitumor activity of ascorbate against Ehrlich ascites tumor cells by the copper:glycylglycylhistidine complex, *Cancer Res. 43*, 824−828.
23. Mack, D. P., and Dervan, P. B. (1990) Nickel-Mediated Sequence-Specific Oxidative Cleavage of DNA by a Designed Metalloprotein, *J. Am. Chem. Soc. 112*, 4604−4606.
24. Mack, D. P., and Dervan, P. B. (1992) Sequence-Specific Oxidative Cleavage of DNA by a Designed Metalloprotein, Ni(II)·GGH-(Hin139−190), *Biochemistry 31*, 9399−9405.
25. Liang, Q., Ananais, D. C., and Long, E. C. (1998) Ni(II)·Xaa-Xaa-His Induced DNA Cleavage: Deoxyribose Modification by a Common "Activated" Intermediate Derived from $KHSO_5$, MMPP, or H_2O_2, *J. Am. Chem. Soc. 120*, 248−257.
26. Long, E. C., and Claussen, C. A. (2004) in *Small Molecule DNA and RNA Binders* (Demeunynck, M., Bailly, C., Wilson, W. D., Eds.) Vol. 1, pp 88−125, Wiley-VCH, Weinheim, Germany.
27. Brittain, I. J., Huang, X., Long, E. C. (1998) Selective Recognition and Cleavage of RNA Loop Structures by Ni(II)·Xaa-Gly-His Metallopeptides, *Biochemistry 37*, 12113−12120.
28. Copeland, K. D., Fitzsimons, M. P., Houser, R. P., and Barton, J. K. (2002) DNA Hydrolysis and Oxidative Cleavage by Metal-Binding Peptides Tethered to Rhodium Intercalators, *Biochemistry 41*, 343−356.
29. Raj, P. A., Edgerton, M., and Levine, M. J. (1990) Salivary histatin 5: dependence of sequence, chain length, and helical conformation for candidacidal activity, *J. Biol. Chem. 265*, 3898−3905.
30. Helmerhorst, E. J., Venuleo, C., Beri, A., and Oppenheim, F. G. (2005) *Candida glabrata* is unusual with respect to its resistance to cationic antifungal proteins, *Yeast 22*, 705−714.
31. Marion, D., and Wuthrich, K. (1983) Application of phase sensitive two-dimensional correlated spectroscopy (COSY) for measurements of 1H-1H spin-spin coupling constants in proteins, *Biochem. Biophys. Res. Commun. 113*, 967−974.
32. Delaglio, F., Grzesiek, S., Vuister, G. W., Zhu, G., Pfeifer, J., and Bax, A. (1995) NMRPipe: a multidimensional spectral processing system based on UNIX pipes, *J. Biomol. NMR 6*, 277−293.
33. Jhonoson, B. A., and Blevins, R. A. (1994) NMRView: a computer program for the visualization and analysis of NMR data, *J. Biomol. NMR 6*, 603−614.
34. Bax, A., and Davis, D.G. (1985) MLEV-17-based two-dimensional homonuclear magnetization transfer spectroscopy, *J. Magn. Reson. 65*, 355−360.
35. Harford, C., and Sarkar, B. (1997) Amino Terminal Cu(II)- and Ni(II)- Binding (ATCUN) Motif of Proteins and Peptides: Metal Binding, DNA Cleavage, and Other Properties, *Acc. Chem. Res. 30*, 123−130.
36. Sigel, H., and Martin, B. (1982) Coordinating properties of the amide bond. Stability and structure of metal ion complexes of peptides and related ligands, *Chem. Rev. 82*, 385−426.
37. Pogni, R., Baratto, M. C., Busi, E., and Basosi, R. (1999) EPR and $O2^{\cdot-}$ scavenger activity: Cu(II)-peptide complexes as superoxide dismutase models, *J. Inorg. Biochem. 73*, 157−165.
38. Nagane, R., Koshigoe, T., and Chikira, M. (2003) Interaction of Cu(II)-Arg-Gly-His-Xaa metallopeptides with DNA: effect of C-terminal residues, Leu and Glu, *J. Inorg. Biochem. 93*, 204−212.
39. Andrade, M. A., Chacon, P., Merelo, J. J., and Moran, F. (1993) Evaluation of secondary structure of proteins from UV circular dichroism spectra using an unsupervised learning neural network, *Protein Eng. 6*, 383−390.
40. Merelo, J. J., Andrade, M. A., Prieto, A., and Morán, F. (1994) Proteinotopic Feature Maps, *Neurocomputing 6*, 443−454.
41. Wishart, D. S., Bigam, C. G., Yao, J., Abildgaard, F., Dyson, H. J., Oldfield, E., Markley, J. L., and Sykes, B. D. (1995) 1H, 13C and 15N chemical shift referencing in biomolecular NMR, *J. Biomol. NMR. 6*, 135−140.
42. Vuister, G. W., Delaglio, F., Bax, A. (1992) An Empirical Correlation between $^{1}J_{C_\alpha H_\alpha}$ and Protein Backbone Conformation, *J. Am. Chem. Soc. 114*, 9674−9675.
43. Manning, M. C., and Woody, R. W. (1991) Theoretical CD studies of polypeptide helices: examination of important electronic and geometric factors, *Biopolymers 31*, 569−586.

44. Beychok S. (1967) Protein Models for Conformational Studies, in *poly-α-Amino Acid* (Fasman, G. D., Ed.) pp 293−337 Dekker, New York.
45. Jin, Y., and Cowan, J. A. (2005) DNA Cleavage by Copper-ATCUN Complexes. Factors Influencing Cleavage Mechanism and Linearization of dsDNA, *J. Am. Chem. Soc. 127*, 8408−8415.
46. Fang, Y. Y., Ray, B. D., Claussen, C. A., Lipkowitz, K. B., and Long, E. C. (2004) Ni(II)·Arg-Gly-His-DNA Interactions: Investigation into the Basis for Minor-Groove Binding and Recognition, *J. Am. Chem. Soc. 126*, 5403−5412.
47. Branum, M. E., Tipton, A. K., Zhu, S., and Que, L., Jr. (2001) Double-Strand Hydrolysis of Plasmid DNA by Dicerium Complexes at 37 °C, *J. Am. Chem. Soc. 123*, 1898−1904.
48. Uma, V., Kanthimathi, M., Subramanian, J., and Unni Nair, B. (2006) A new dinuclear biphenylene bridged copper(II) complex: DNA cleavage under hydrolytic conditions, *Biochim. Biophys. Acta 1760*, 814−819.
49. Brewer, D., and Lajoie, G. (2002) Structure-Based Design of Potent Histatin Analogues, *Biochemistry 41*, 5526−5536.
50. Bal, W., Wojcik, J., Maciejczyk, M., Grochowski, P., and Kasprzak, K. S. (2000) Induction of a Secondary Structure in the N-terminal Pentadecapeptide of Human Protamine HP2 through Ni(II) Coordination. An NMR study, *Chem. Res. Toxicol. 13*, 823−830.
51. Beese, L. S., and Steitz, T. A. (1991) Structural basis for the 3′-5′ exonuclease activity of *Escherichia coli* DNA polymerase I: a two metal ion mechanism, *EMBO J. 10*, 25−33.
52. Ma, L., Tibbitts, T. T., and Kantrowitz, E. R. (1995) *Escherichia coli* alkaline phosphatase: X-ray structural studies of a mutant enzyme (His-412→Asn) at one of the catalytically important zinc binding sites *Protein Sci. 4*, 1498−1506.
53. Baev, D., Li, X. S., Dong, J., Keng, P., and Edgerton, M. (2002) Human salivary histatin 5 causes disordered volume regulation and cell cycle arrest in *Candida albicans*, *Infect. Immun. 70*, 4777−4784.

BI0615137